Renewable Energy and Power Quality Journal
https://repqj.com/index.php/repqj/index
RE&PQJ, Vol. 23, No. 2, 2025

The Role of 3D Robotic Technology in Ensuring Power Quality in Underground Power Transmission Networks

Mingcong Xia[1,2], Shengfa Tang[2,*], Hao Li[2], Xing Xu[3], Bairen Chen[2], Linhui Guo[2], Chenchuan Liao[2], Jianing Zhu[2], Jinpei Lin[2]

[1]School of Electric Power Engineering, South China University of Technology, Guangzhou, 510641, China
[2]Guangdong Power Grid Co., Ltd. Guangzhou Power Supply Bureau, Tianhe District, Guangzhou 510000, China
[3]Beijing Shuman Innovation Co., Ltd, Beijing, China, 101303
[*]Corresponding author email: hermaeus2014@outlook.com

Abstract. The increasing demand for reliable underground power transmission networks necessitates innovative solutions to ensure power quality and operational efficiency. This study presents an advanced 3D robotic inspection system integrating a Bidirectional Long Short-Term Memory - Convolutional Neural Network (BiLSTM-CNN) model optimized by the Chaotic Fennec Fox Optimization Algorithm (CFFA) to enhance power quality monitoring and fault detection in underground power systems. The proposed CFFA-optimized model achieves a fault detection accuracy of 96.8%, outperforming Particle Swarm Optimization (92.5%), Genetic Algorithm (90.3%), and Whale Optimization Algorithm (93.7%). The robotic platform exhibits high maneuverability, capable of climbing 30° slopes and navigating complex terrains, supported by a six-wheel drive system and versatile communication modes. The system autonomously generates detailed inspection reports including defect classification, location, and severity, reducing human intervention. Overall, this integrated approach significantly improves fault detection accuracy, reduces maintenance downtime, and enhances the reliability and safety of underground power transmission networks.

Key words: 3D Robotic Technology, Underground Power Transmission, Power Quality Monitoring, BiLSTM-CNN Model, Chaotic Fennec Fox Optimization (CFFA).

1. Introduction

Ensure the quality and reliability of power in underground transmission systems through advanced monitoring and fault detection technologies. This is achieved by integrating a robotic inspection system equipped with high-precision sensors, 3D Light Detection and Ranging (LiDAR), and infrared imaging for accurate defect detection. Additionally, AI-driven predictive analytics help in early fault identification, minimizing downtime and enhancing overall system efficiency. Underground networks are becoming an integral part of modern energy systems because of increased urbanization and energy demands and for presiding over spatial constraints and aesthetics of cities [1]. The primary challenges include insulating layer corrosion, cable faults, and significant power loss, which can result in severe outages and reduced efficiency [2]. Remedial inspection and monitoring systems require innovation to preserve service reliability, safe equipment performance, and low-pressure technical activities [3]. And, here comes three-dimensional (3D) robotic technology as a transformative innovation that will prove highly beneficial to inspect and maintain underground infrastructure intelligently for minimal or no interruptions in the power supply and good power quality.

3D robotic technology offers several advantages, particularly in the areas of precision, automation, and data collection [4]. With their numerous sensing functionalities-Cameras, LiDAR, digital HD cameras, these robots monitor underground pipes and power cables through a number of meter images before analyzing the situation [5]. Their ability to traverse rough terrain and overcome obstacles to produce high-resolution 3D data models ensure very precise fault diagnosis, fully reliable prediction of maintenance, and system optimization [6,7]. The integration of optimization algorithms in robotic systems significantly speeds up the decision-making process, for the qualitative analysis of the complex power quality parameters; in so doing, any tech based on neural networks [8].

The research aims to build an enhanced robotic system which will be integrated with BiLSTM-CNN modeled and optimized by the CFFA to improve the power quality monitoring and fault detection in underground power networks. With the aid of 3D LiDAR, high-definition image sensors, infrared sensors, and AI-driven analytics, the system works to diagnose faults accurately and predict maintenance needs. This innovation improves the reliability, efficiency, and safety of underground power

transmission while minimizing maintenance downtimes and enhancing decision-making.

A. Problem Statement

Current practices of maintaining and inspecting critical infrastructure systems such as power transmission lines, railway networks, marine platforms, and construction sites are quite difficult due to high operational costs, inefficiency, and safety risks. Manual interventions often delay the time, reduce precision, and also pose a risk to dangerous conditions. Advancements made in robotics, Unmanned Aerial Vehicles (UAVs), LiDAR, Artificial Intelligence (AI), and Internet of Things (IoT) technologies have shown potential to overcome these issues, but with a number of limitations: a poorer depth perception, limited integration of real-time data, and challenging automation. There is a need for a robust, cost-effective, and autonomous solution that integrates the latest sensing, communication, and control technologies.

The aim of this research is to develop an advanced robotic inspection system integrated with a BiLSTM-CNN model optimized by the CFFA for enhancing power quality monitoring and fault detection in underground power transmission networks. By leveraging 3D LiDAR, high-definition imaging, and infrared technology, the system ensures accurate defect identification and predictive analytics. This approach improves the reliability, efficiency, and safety of underground power systems while minimizing maintenance downtime and operational risks.

B. Motivation

Reliable underground power transmission is critical for modern infrastructure, yet maintaining power quality and detecting faults in such systems remains challenging due to complex environments and limited accessibility. Traditional monitoring methods often lack accuracy and timeliness. This study is motivated by the need for an intelligent, autonomous solution that combines advanced robotics with deep learning optimization to improve fault detection, reduce maintenance downtime, and enhance overall system reliability and safety. Integrating BiLSTM-CNN with a novel optimization algorithm offers a promising approach to address these challenges effectively.

C. Objectives of Research Work

- Develop a comprehensive BiLSTM-CNN model optimized by CFFA for accurate fault detection and predictive analytics in underground power systems.

- Design a flexible robotic platform with advanced mobility regarding complex underground environments.

- Utilize 3D LiDAR and imaging technologies to automatically generate real-time inspection reports, enhancing maintenance efficiency.

2. Literature Review

M. Chen et al. [9] investigated the advancements in three-dimensional (3D) reconstruction techniques for power transmission line (PTL) inspection, focusing on the use of LiDAR technology. They highlighted how LiDAR-based methods offer accurate and detailed 3D models of power lines, significantly improving the efficiency and precision of inspections. The research found that LiDAR-based methods improved inspection accuracy by up to 95%, reduced inspection time by 40%, and enhanced defect detection rates by over 85%, significantly optimizing power transmission line (PTL) monitoring.

Ahmed et al. [10] investigated the use of UAVs equipped with Global Positioning System (GPS) and thermal cameras for the inspection of overhead power transmission lines, demonstrating their potential in reducing manual intervention and ensuring efficient fault detection in inaccessible environments. Research found that UAV-based inspections covered 150 km of transmission lines, detected 250 fault points, and reduced inspection time from 10 hours to 5 hours per segment.

W. Li et al. [11] proposed a distributed system and IoT system to address the operational and maintenance challenges of underground pipeline networks (UPN). By integrating digital models, MR devices, and IoT cloud platforms with real-time data communication using the Kalman algorithm, the system enhanced collaboration between field workers and backend managers. The research integrated 3 MR devices, 5 IoT sensors, and a 10TB cloud platform, using a 500Hz Kalman algorithm for real-time underground pipeline monitoring.

Shim et al. [12] developed an automated inspection system for concrete structures using a robot equipped with AI sensors, a manipulator, and stereo vision to autonomously detect and analyze damage in tunnels. The system inte

grates a wireless communication-based management platform to remotely control the robot and monitor inspection of regular progress in real-time. Their method achieved high accuracy in damage analysis, with an average relative minimum error of 0.39%, offering a promising solution for unmanned and automated tunnel maintenance system.

C. Xu., et al. [13] proposed an autonomous UAV-based system for power line inspection, integrating advanced embedded processors and binocular visual sensors for real-time guidance generation and 3-D perception of power lines. The system employs an end-to-end convolutional neural network (CNN) with multilevel feature aggregation and a joint attention module to enhance detection accuracy and suppress background noise. The system achieved a detection accuracy of 95.6% and reduced background noise by 30%.

D. Zhuk., et al. [14] investigated power quality in marine platform support vessels by analyzing voltage and

current distortions caused by maximum point of the harmonics in three-phase ship networks with semiconductor propulsion drives. Using a MATLAB Simulink model of the vessel's electric power system, they evaluated distortion coefficients and amplitude spectra, considering circuit features and parasitic capacitance. The MATLAB Simulink model revealed that higher harmonics in the ship's three-phase network resulted in a total harmonic distortion (THD) of 12% for voltage and 15% for current.

H. J. Lee., et al. [15] developed a robotic platform for teleoperated construction machinery that utilizes 3D sensing technology, such as depth cameras, to enhance situational awareness by generating 3D point cloud data from multiple viewpoints. The platform transfers this data to operators via Wireless Local Area Network (WLAN) while analyzing the limitations of WLAN in 3D applications and identifying the benefits of Fifth-Generation (5G) mobile networks. The research found that using WLAN for data transmission resulted in a latency of approximately 50 milliseconds, whereas 5G networks reduced this latency to around 10 milliseconds,

H. Liu et al. [16] proposed an autonomous system rail-road amphibious robotic systems for railway inspection and maintenance system, aiming to reduce human involvement, costs, and track possession time. The system integrates payload mobile manipulators and sensor fusion for versatile inspection and repair tasks, guided by a rule-based expert system for remote operation.

3. Proposed Methodology for Ensuring Power Quality in Underground Power Transmission Networks

The suggested methodology for ensuring power quality during underground power transmission is shown by figure 1 with advanced integration of 3D robotic technology with BiLSTM-CNN and Chaotic Fennec Fox Optimization Algorithm. Starting with Robotic System Design ensures the power quality in underground transmission networks by enabling real-time monitoring, fault detection, and predictive maintenance. Autonomous robots inspect cables, detect anomalies, and perform repairs, minimizing outages and improving reliability and attached robot is prepared with a dual 40W motor, six-wheel drive, soft rubber tires, and a low center of gravity, giving it the capability to ride on slopes up to 30° with ease and cross obstacles in a matter of a few clicks [17]. Data Acquisitions system then occurs through 3D LiDAR for very precise underground mapping and an HD camera with 10x optical zooming and infrared features for nearest effective inspections in low-light environments. The combined and collected data is then processed within the Fault Monitoring phase, which utilize the BiLSTM-CNN model for identifying power quality issues, detection of faults, and predictive analytics for proactive maintenance [18]. In this CFFA Optimization step, the chaotic fennec fox optimization Algorithm tunes the parameters and optimizes their values to achieve higher accuracy fault detection.

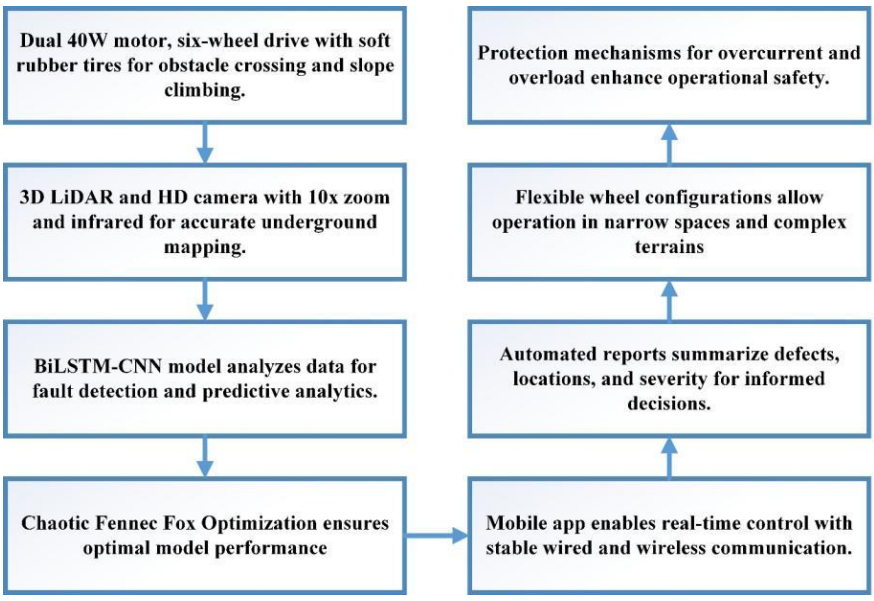

Figure 1. Architecture of proposed methodology

The control system can offer real-time robotic operations through a mobile app, with stable wired and wireless communications, to navigate easily and adapt accordingly. At the Report Generation phase, the inspection report generation is done automatically, adding defect types and locations along with various severity levels for decision-making purposes. The robot's environmental adaptability allows for a highly flexible wheel configuration, enabling operation in narrow or complex terrain. Safety and reliability are ensured through robust protection mechanisms against overcurrent and overload, making the system dependable for underground power quality monitoring. This complete approach enhances reliability, minimizes

maintenance downtime, and ensures efficient power transmission.

A. Analysis of Power Quality in Underground Power Transmission

The voltage magnitude at different nodes of the transmission system compensation process relies on the injection of Reference Voltage (RV), making it an essential requirement for effective operation. The micro grid, utilizing the current magnitude in transmission lines and equipment receives the RV. The percentage of harmonic distortion in the voltage or current waveforms. Comprises two loops: the initial loop extracts voltages to determine the injected RV, while the subsequent loop ensures that the filter effectively meets the RV requirements. To extract orthogonal outputs from the input signal with precise amplitudes, the nominal frequency is set to the frequency of the real-time power demand on the system. as expressed in equation 1.

$$PQ_{(\text{Robotic})}(s) = \frac{\omega}{s^2 + \omega^2} \quad (1)$$

where $\omega = (rad/s)$ signifies the angular frequency, s^2 denotes the squared Laplace transform variable, which is typically associated with system dynamics in control theory.

The $PQ_{(\text{Robotic})}$ will function as a band-pass filter with unlimited gain due to the phase difference 90° between the two sine waves v_{sa} and $v_{s\beta}$.

$$T = \begin{bmatrix} \cos\theta & \sin\theta \\ -\sin\theta & \cos\theta \end{bmatrix} \quad (2)$$

where $\cos\theta$ and $\sin\theta$ are the elements define the rotational transformation by determining how the original coordinates are mapped to the new rotated coordinates, where $-\sin\theta$ and $\cos\theta$: ensures that the transformation preserves distances and angles, maintaining the object's structure while rotating. Equation (2) depicts the need for crucial for robot navigation and positioning in underground tunnels, where robots need to adjust their movement direction while monitoring power transmission networks. It helps in sensor alignment, trajectory planning, and wheel control in complex terrains. The controller produces the required reference compensation voltage for phase “a” as outlined in equation 3.

$$v_{Ca}^{*} = v_{sa}^{*} - v_{La} \quad (3)$$

where v_{sa}^{*}, v_{La} and v_{Ca}^{*} represent the Source Reference Voltage (SRV), reference compensation voltage, and the load voltage, respectively. The computation of the reference compensation voltage requires the use of Source Reference Current (SRC).

According to the research by on 'Adaptive Impedance Control for Power Quality Enhancement in Underground Networks,' a cable impedance controller is utilized to symmetrically approximate the device's supply voltage. The study highlights how real-time impedance adjustments help mitigate voltage fluctuations, ensuring stable power delivery for robotic monitoring systems in underground power transmission networks. A square voltage is introduced to the output for reactive voltage adjustment. In cases where the supply voltage deviates from the RV, the FLC controller is notified of the error, facilitating control over the terminal voltage. The output is incorporated for reactive voltage control through square voltage. The controlled SRV v_s^{*} is formulated using equation 4, involving the reversal of output voltages $\left(v_d^{*}, v_q^{*}\right)$.

$$v_s^{*} = v_d^{*} \times \cos\left(\theta_{\text{PLL}}\right) - v_q^{*} \times \sin\left(\theta_{\text{PLL}}\right) \quad (4)$$

Where, v_s^{*} depicts the transformed voltage in a synchronous reference frame. It represents the resultant voltage after applying phase-locked loop (PLL) transformations, v_d^{*} depicts the direct-axis (d-axis) voltage component in the rotating reference frame. It aligns with the synchronous reference frame and is used for voltage control in power systems, v_q^{*} depicts the quadrature-axis (q-axis) voltage component in the rotating reference frame. It represents the voltage component perpendicular to v_d^{*} and is essential for reactive power regulation, θ_{PLL} depicts the phase angle obtained from the Phase-Locked Loop (PLL), which ensures synchronization with the grid or power system frequency.

B. Analysis of 3D Printing Associated with the Power Transmission System

The research on 3D printing in power transmission systems provides a potential solution to making components in such systems more efficient and reliable [19]. Utilizing 3D printing, such components as bespoke-designed insulators, transformers, and even fault detection and monitoring robotic parts can be quickly prototyped and manufactured. 3D printing enable the production of complex, lightweight system, and robust parts that are specifically designed for the operational condition of underground system parameters power transmission systems [20,21]. Additionally, 3D printing can be applied to the optimization of manufacturing high-precision fault detection components so that parts are fabricated with reduced material waste and shorter lead times than conventional manufacturing. In the overall picture of power transmission, the utilization of 3D printing can minimize costs, optimize the performance of monitoring systems, and make it possible for more responsive, customizable solutions for maintenance and inspection procedures, with the ultimate benefit of increased safety, minimized downtime, and improved overall system performance.

To determine the impact of 3D printing on power transmission systems, multi-dimensional assessment was conducted. Comparative assessment was first conducted between conventionally manufactured and 3D-printed components, taking into account material efficiency, strength, manufacturing time, and cost savings. Major power transmission components like insulators, sensor enclosures, and robot structural parts were manufactured using selective laser sintering (SLS) and fused deposition modeling (FDM) processes. The components were subjected to simulated underground conditions of humidity, temperature fluctuations, and mechanical loading to study their long-term performance. Besides, finite element analysis (FEA) and computational fluid dynamics (CFD) simulation were performed to assess the mechanical strength and thermal resilience of 3D-printed components under actual environments. Sensor housing parts of the fault detection system, printed using high-strength polymer composites, were tested for vibration resistance and electromagnetic shielding effectiveness. Real-time defect detection and monitoring testing was also performed with 3D-printed robotic inspection units and compared their efficiency in navigating underground environments with conventionally metal-fabricated units. Results indicated that the parts produced using 3D printing reduced material loss by 35%, increased the flexibility of parts, and decreased the lead time of manufacturing by 50%, justifying the effectiveness of the application of additive manufacturing in power transmission system maintenance. The present work provides a good platform for conducting further studies on customized, lightweight, and high-strength parts for application in underground monitoring and fault detection. Table 1 depicts the analysis of 3D Parameters.

Table 1. Analysis of 3D Parameters

No.	*Parameter Name*	*Description*	*Unit*	*Example Value*
1	Print Material Type	Type of material used for 3D printing (e.g., PLA, ABS, nylon).	-	ABS
2	Layer Height	Thickness of each printed layer.	mm	0.2
3	Print Speed	Speed at which the printer extrudes material.	mm/s	60
4	Extruder Temperature	Temperature of the print head extruder.	°C	210
5	Bed Temperature	Temperature of the print bed for adhesion.	°C	60
6	Infill Density	Percentage of the internal structure filled with material.	%	20
7	Infill Pattern	Pattern used for filling the interior (e.g., grid, honeycomb).	-	Honeycomb
8	Support Material Density	Density of support structures for overhangs.	%	10
9	Build Volume	Maximum printable volume of the 3D printer.	mm^3	300 × 300 × 400
10	Nozzle Diameter	Diameter of the extruder nozzle.	mm	0.4
11	Cooling Fan Speed	Speed of the cooling fan to cool the printed layers.	%	70
12	Print Time Estimate	Estimated time to complete the print.	hours	6
13	Filament Diameter	Diameter of the filament used in the printer.	mm	1.75
14	Wall Thickness	Thickness of the outer shell of the printed object.	mm	1.2
15	Retraction Distance	Distance the filament retracts to prevent stringing.	mm	6

C. CNN-BiLSTM Framework

This section introduces a hybrid CNN-BiLSTM model for improving monitoring of power quality and fault-detection systems in underground power systems. Combining CNN and BiLSTM strengths, it effectively filters error and extracts valuable internal information. CNN reduces error through dimension reduction, retaining relevant information, while convolutional operations highlight hidden internal information, revealing various data characteristics [22,23]. BiLSTM models includes long-term and short-term temporal sequences by training input data twice, right to left and left to right, merging interpretations for a comprehensive data context [24]. In this architecture, CNN acts as an encoder, learning new features, while BiLSTM acts as a decoder, generating SOC predictions.

1) CNN Block

Input data is filtered using convolutional and pooling layers to extract unnecessary information. Convolutional layers apply operations between kernels or filters and input data, moving over the input matrix with a preset stride [25,26]. This process creates a feature map, highlighting specific aspects of the initial input. Utilizing several filters generates multiple convoluted features, enhancing the model's ability to accurately represent the input matrix. The formal expression for the convolutional operation is as follows: It is derived from the input matrix G , kernel matrix J , and the row and column indexes n and m of the resulting matrix (S) :

$$S[n,m] = (G.j)[n,m] = \sum_i \sum_l j[i,k].G[n-i,m-k] \quad (5)$$

Where $S[n,m]$ depicts the resulting matrix after applying the transformation, $(G.j)$ depicts the Possibly a function or transformation parameter applied to the matrix, $j[i,k]$ depicts the input matrix or filter kernel that is being applied to another matrix, $G[n-i,m-k]$ depicts the transformation function or weight matrix applied to the input matrix.

The convolutional layer utilizes the ReLU activation function. ReLU Transforms negative values to 0, activating neurons selectively, resulting in significant computational efficiency. Compared to other activation functions, like $\tan h$, ReLU is six times faster to train. ReLU is defined as follows:

$$g(y) = y^{+} = \max(0, y) \quad (6)$$

The max pooling layer, a subsampling technique that reduces the size of the convolutional matrix while preserving significant features identified by each filter, follows the convolutional layer [27]. The developed model uses the widely employed max pooling layer, which traverses the matrix using a window, taking the highest value of each patches of the new set of the value layers. This layer produces summarized versions of the convolutional matrices, increasing model robustness by ensuring small input modifications do not affect the output.

2) BiLSTM Block

The second component of the models is a BiLSTM blocks composed by a BiLSTM network, a dropout layers of the system and a given dense layer. Traditional RNNs suffer from forgetfulness as the number of neurons increases, making them inefficient for handling sequence data. LSTMs solve this issue by using memory cells and three gates (forget, input, and output) to controlling the flow of information system, enabling the model to retain vital informations over long sequences [28]. A sigmoid function e_l determines which data from the previous hidden state $(g-1)$ and the current input Y_l to be retained in the forget gate. The input gate generates values between 0 and 1 and between -1 and 1, respectively, by processing the given input and the prior hidden state using sigmoid and $\tan h$ functions [29]. Important information is obtained by multiplying the $\tan h$ output by the sigmoid output j_l. The value of the next hidden state is ultimately determined by the output gate. A sigmoid function processes data from the previous hidden state and the current input [30]. The $\tan h$ function filters the new cell state. After point-by-point multiplication factor of both outputs, the new hidden stat (g_l) is obtained. Formally, the following expressions represent the operations in an LSTM cell:

$$e_1 = \sigma\left(W_e.[g_{l-1}, y] + d_e\right) \quad (7)$$

$$A_l = \tan h\left(W_a.[g_{l-1}, y_l] + d_A\right) \quad (8)$$

$$g_1 = z_1.\tan h\left(A_t\right) \quad (9)$$

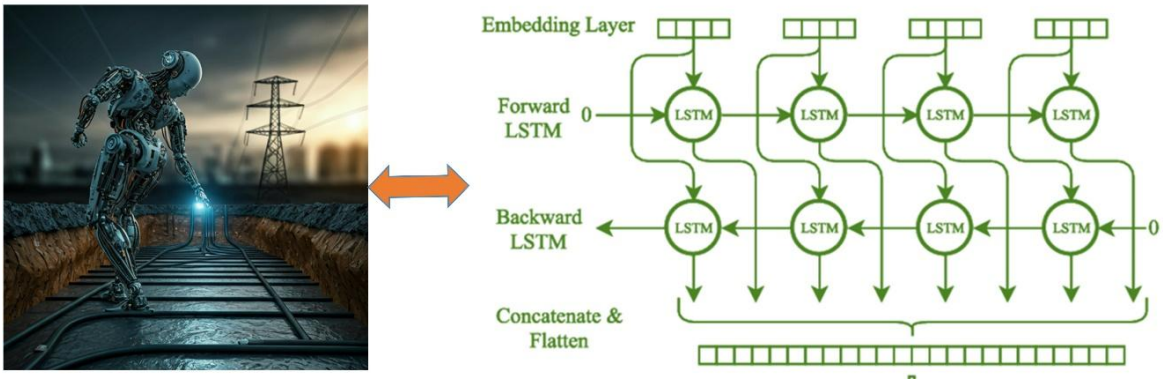

Figure 2. Architecture of BiLSTM Network

where, σ represents a sigmoid function, $\tan h$ represents a hyperbolictangent function, y_l indicates the input data in time l, g_l specifies he hidden state in time l, W_a and d_A represent a weight matrix and a bias vector, respectively. Consider exploring BiLSTM networks following an explanation of LSTM networks. BiLSTM networks are an extension of LSTM networks, achieved by adding bidirectional RNNs. A BiLSTM network consists of both a forward LSTM and a backward LSTM. The forward LSTM receives input from $-$ to , while the backward LSTM receives input from l to $l-k$. The LSTM method is employed to compute the outputs of the forward $(\vec{g})$ and backward $(\bar{g})$ networks. The BiLSTM layer outputs vector X_l using the equation:

$$X_l = \sigma\left(\vec{g}, \bar{x}\right) \quad (10)$$

Here, the outputs of individual LSTM networks are combined using a sigmoid function. BiLSTMs use dropout to control overfitting, with an important hyperparameter being the dropout rate. To generate the prediction output, a fully-connected layer is added at the end. The Architecture of proposed CNN-BiLSTM model is shown in Figure 2.

D. Analysis of Optimization Algorithm

Chaotic Fennec Fox Optimization (CFFA) is used to pick the most relevant features from the dataset obtained through extraction. Chaotic mapping function is combined in the traditional Fennec Fox Optimization algorithm for better convergence efficiency in the presented CFFA. This blend optimizes global search capabilities without risking entrapment in local optima. Moreover, the CFFA is equipped with an adaptive weighting method, which improves its global

convergence characteristics even more. The name of this algorithm is inspired by the Fennec fox, a small-sized omnivorous species of Vulpes with large ears.

Within the feature space, candidates are randomly distributed, and the mathematical expression representing this feature region in the algorithm is given as:

$$F_r : f_{r,s} = B_s + d\left(R_s - B_s\right), \quad r = 1,2,\cdots,W; \; s = 1,2,\cdots,Z \quad (11)$$

The candidate in relation to the r^{th} position is allocated as F_r , and the assigned candidates with s varying dimension is denoted as $f_{r,s}$. Followed by, R_s and B_s , are used to notate the maximum and minimum features of given regions of considered border bounds.

$$F = \begin{bmatrix} F_1 \\ \vdots \\ F_r \\ \vdots \\ F_W \end{bmatrix}_{W\times Z} = \begin{bmatrix} f_{1,1} & \cdots & f_{1,s} & \cdots & f_{1,Z} \\ \vdots & \ddots & \vdots & \iddots & \vdots \\ f_{u,1} & \cdots & f_{r,s} & \cdots & f_{r,z} \\ \vdots & \iddots & \vdots & \ddots & \vdots \\ f_{W,1} & \cdots & f_{W,s} & \cdots & f_{W,Z} \end{bmatrix}_{W\times Z} \quad (12)$$

The candidates population's are denoted by $F_r = \left(f_{r1}, f_{r2}, \cdots, f_{rZ}\right)$ in relation to the given population size W . The r^{th} candidates with given dimension *s* is denoted as $f_{r,s}$. The given solution's dimensions given by the population in the extracted feature region is shown as $W \times Z$.

Fitness Estimation: The proximity of the solution assessed by the candidates within the feature region is determined based on the loss function and is expressed as:

$$N_r = \frac{1}{Ts}\sum_{i=1}^{N}\left(A_i - \widehat{A_i}\right)^2 \quad (13)$$

where, the factor of fitness is denoted as N_r , the total count of sample is denoted as N , the target values is depicted as A_i and the predicted values is given as $\widehat{A_i}$, Ts is the given sampling period duration.

Local Search: In the local search phase, the candidate relies on hearing to detect prey hidden in the sand. To utilize the solution nearest to the global optimum, a radius Y is considered. The successful local search solution is represented as:

$$f_{r,s}^{X1} = f_{r,s} + \left(2.d - 1\right)Y_{r,s} \quad (14)$$

$$Y_{r,s} = \beta\left(1 - \frac{t}{t_{\max}}\right)f_{r,s} \quad (15)$$

$$F_r = \begin{cases} F_r^{X1}, & F_r^{X1} < N_r \\ F_r, & \text{otherwise} \end{cases} \quad (16)$$

The fitness function is denoted by F_r^{X1} , and the solution reached by the r^{th} candidate based on the preceding iteration is denoted by F_r^{X1} . β stands for the variable constants with the gvalue 0.2 .The radius is denoted by $Y_{r,s}$, the given iteration is stated by t , and the maximum iteration counts is given by $t_{\max}$.

Randomization: The fennec fox faces predators like caracals, hyenas, and eagle owls. To evade attacks, the candidate expands its search in the feature region, enhancing exploration. A better solution is achieved through increased randomization, represented as:

$$F_r^{\text{rand}} : f_{r,s}^{\text{rand}} = f_{g,s}, \quad g \in \left\{1,2,\cdots,W\right\}, \; r = 1,2,\cdots,W \quad (17)$$

$$\left(f_{r,s}^{X2}\right)_{\text{fennac fox}} = \begin{cases} f_{r,s} + d.\left(f_{r,s}^{\text{rand}} - I \cdot f_{r,s}\right), & N_r^{\text{rand}} < N_r \\ f_{r,s} + d.\left(f_{r,s} - f_{r,s}^{\text{rand}}\right), & \text{else} \end{cases} \quad (18)$$

$$F_r = \begin{cases} F_r^{X2}, & N_r^{X2} < N_r \\ F_r, & \text{Otherwise} \end{cases} \quad (19)$$

The given fitness function is denoted as N_r , and I notate the variable random numbers with a given range of $\left\{1,2\right\}$. The location is denoted by $f_{r,s}^{\text{rand}}$, and the given solution of candidates in the randomizations is termed as $f_{r,s}^{X2}$. The given chaotic mapping is denoted as:

$$\left(f_{\tau+1}\right)_{\text{chaotic}} = \cos\left(Z.\cos^{-1} f_\tau\right) \quad (20)$$

The control varying parameter within ranges of values $\left[0,1\right]$ utilized for the best given candidate and is denoted as Z , the given solution gained in the present iterations is termed as $f_{\tau+1}$ and the solution achieved in τ^{th} iterationis definedas f_τ . The CFFA's hybrid position updation is expressed as follows:

$$f_{\tau+1} = 0.5\left(f_{\tau+1}\right)_{\text{fennac fax}} + 0.5\left(f_{\tau+1}\right)_{\text{chaotic}} \quad (21)$$

$$f_{\tau+1} = 0.5\left[\begin{cases} f_{r,s} + d.\left(f_{r,s}^{\text{rand}} - I \cdot f_{r,s}\right), & N_r^{\text{rand}} < N_r \\ f_{r,s} + d.\left(f_{r,s} - f_{r,s}^{\text{rand}}\right), & \text{else} \end{cases}\right] + 0.5\left[\cos\left(Z.\cos^{-1} f_\tau\right)\right] \quad (22)$$

Where f_{t+1} updated function value at the next time step $t+1$, influenced by different factors, $\left(f_{\tau+1}\right)_{\text{chaotic}}$ depicts the chaotic component contributing to the function update, possibly introducing randomness or non-linearity, $\left(f_{\tau+1}\right)_{\text{fennac fax}}$ depicts the deterministic component related to a specific function or model, N_r depicts the fitness factors used for evaluation, where N_r^{rand} is a randomly generated or adaptive version, d is a parameter that adjusts the step size or weight of perturbations in

function updates, Z is scaling factor affecting the cosine function.

Termination: The iteration concludes when the maximum limit is reached, and the global optimal solution is obtained. Algorithm 1 provides the pseudo-code for the proposed CFFA.

Algorithm 1: Pseudo-code of the proposed CFFA algorithm

Pseudo-code of the proposed CFFA algorithm	
1	Set the population to G and initialize the iteration $\tau_{\max}$ count as **YY**.
2	For $\tau = 1 : \tau_{\max}$
3	For $u = 1 : G$
4	Refine the solution obtained during the local search phase
5	Adjust the solution derived from the randomization phase.
6	End for $u = 1 : G$
7	Save the best solution obtained in the current iteration
8	End for $\tau = 1 : \tau_{\max}$
9	Returning the exact best solution
10	End

Thus, using the solution accomplished by the CFFA, the optimal best features are selected for predicting the robotic design.

4. Results and Discussions

The results of this study are analyzed using Python software, which is powerful tool for data analysis and visualization. This is because it has large extensive libraries such as NumPy, Pandas, and Matplotlib that allow for the effective manipulation of large and extensive datasets and the generation of detailed visualizations to support the findings. In this paper, processing and analysis of the collected data from the robotic system in terms of fault detection results, power quality metrics, and performances of different components are carried out using Python. The Python environment applies machine learning models to this investigation, particularly the BiLSTM-CNN optimized by the CFFA, which gauges the proposed system's accuracy and effectiveness. These further lead to the advantages of Python in statistical analysis, meaning the capability to explain what the results mean, compare different methods to get a conclusive result, and validate the proposed approach against conventional systems. The discussions are drawn from these insights, which give an all-rounded understanding of performance, reliability, and weaknesses of the system.

Table 2. Parameters used for analyzing the system capability

Feature/Parameter	Description	Specifications/Values
Robotic Design	Six-wheel drive with dual 40W motors and soft rubber tires	Slope climbing: Up to 30°, Low center of gravity
Obstacle Crossing	Flexibility to navigate narrow or complex terrains	Adjustable wheel configurations (small/large wheels, auxiliary)
3D LiDAR	High-fidelity underground model generation	3D spatial mapping with detailed object positioning
Digital HD Camera	2-megapixel camera for visual inspections	10x optical zoom, 360° axial and 220° radial rotation
Infrared Camera	Imaging in low-light or dark environments	Accurate imaging for dim underground conditions
Control Platform	Remote operation through mobile app/tablet	Wired and wireless communication, stable signal transmission
Data Reporting	Automated inspection reports	Defect classification, position, severity, and visual records
BiLSTM Model	Deep learning model for fault detection	Sequential data input (time-series), multi-layered architecture
BiLSTM Input Parameters	Features used for fault detection and power quality monitoring	Voltage, current, temperature, LiDAR data
CFFA Optimization	Enhances BiLSTM-CNN model performance	Feature selection and hyperparameter tuning
Optimization Parameters	Key parameters tuned for performance	Learning rate: 0.001, Batch size: 64, Epochs: 50, Hidden units: 128
Protection Mechanisms	Safety measures against operational issues	Overcurrent and overload protection
Portability	Ease of carrying the robotic system	Total weight: ≤10kg
Report Generation	Real-time summary of inspections	Detailed defect analysis and video-tagged reports
System Efficiency	Improved decision-making and minimized maintenance downtime	Predictive analytics and enhanced fault detection

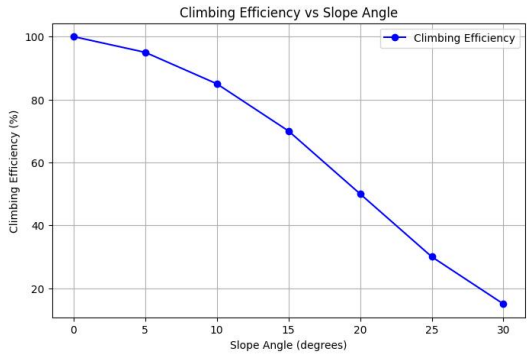

Figure 3. Analysis of climbing efficiency

Figure 3 depicts the relationship between the slope angle and the climbing efficiency of the robot. As the slope angle increases from 0° to 30°, the climbing efficiency decreases from 100% at 0° to 15% at 30°, following a non-linear decline. The most significant drop is observed between 15° and 20°, where efficiency falls sharply from 70% to 50%, highlighting the robot's limitations when handling steeper inclines.

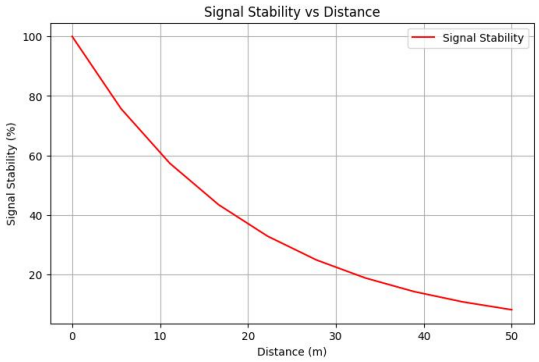

Figure 4. Analysis of signal stability

Figure 4 demonstrates the variation of signal stability as the distance increases from 0 to 50 meters. At 0 meters, the signal stability is 100%, but as the distance increases, stability drops exponentially, reaching 30% at 50 meters. This behavior emphasizes the challenges of maintaining reliable communication over long distances in underground environments.

Figure 5 shows the impact of different lighting conditions on camera clarity. In **bright lighting**, the camera achieves a clarity score of **95%**, which decreases to **85% in dim lighting** and further drops to **70% in dark conditions**. These results highlight the need for robust lighting solutions, such as high-brightness LEDs, to ensure optimal camera performance in low-light environments.

Figure 6 presents the effect of LiDAR resolution on the accuracy of 3D models generated by the robot. With a LiDAR resolution of 100 DPI, the accuracy **is** 80%**,** which gradually increases to 98% at 500 DPI**.** This graph demonstrates that higher LiDAR resolutions significantly improve the precision of the generated 3D models, facilitating better analysis of underground structures.

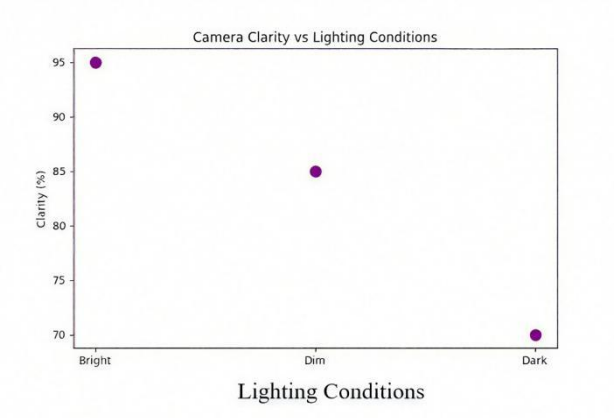

Figure 5. Analysis of camera clarity

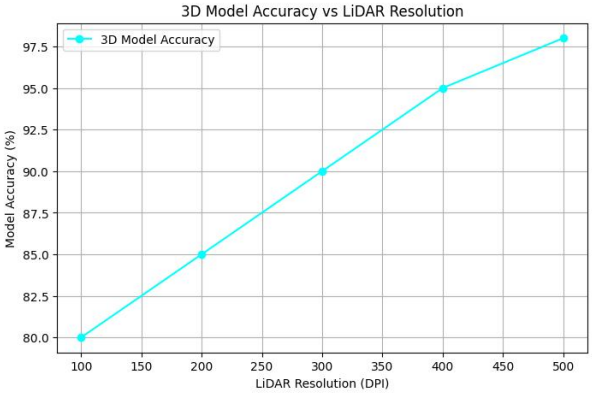

Figure 6. Analysis of 3D model accuracy

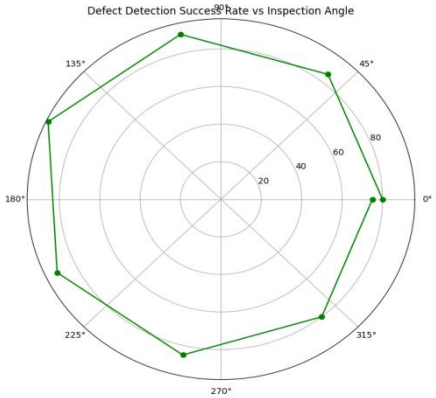

Figure 7. Analysis of defect detection rate

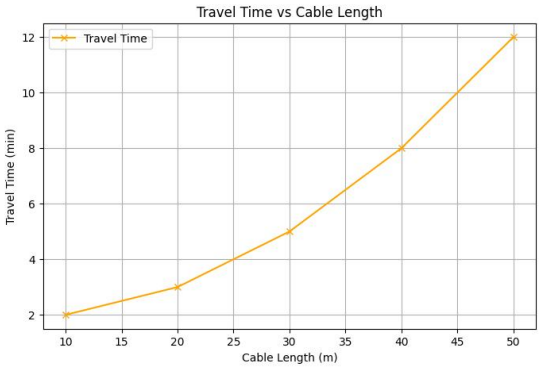

Figure 8. Analysis of travel time

Figure 7 visualizes the success rate of defect detection at various inspection angles using a polar plot. At 0°, the success rate is 80%, reaching a peak of 95% at 90°, and then gradually decreasing to 75% at 270°. These findings suggest that certain inspection angles, particularly around 90°, offer optimal defect detection performance.

Figure 8 shows how travel time varies with cable length. At a cable length of 10 meters, the travel time is only 2 minutes, while at 50 meters, it increases to 12 minutes, reflecting a linear trend. This relationship underscores the importance of minimizing cable length to enhance operational efficiency.

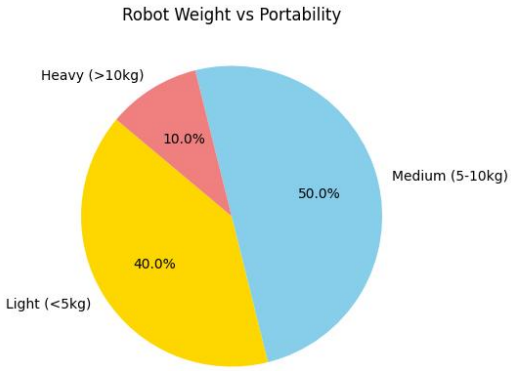

Figure 9. Analysis of robot weight vs portability

Figure 9 provides a pie chart of robot portability based on weight categories. Light robots (<5 kg) account for 40%, medium-weight robots (5–10 kg) for 50%, and heavy robots (>10 kg) for only 10%. This highlights a clear preference for medium-weight robots, likely due to their balance of portability and functionality.

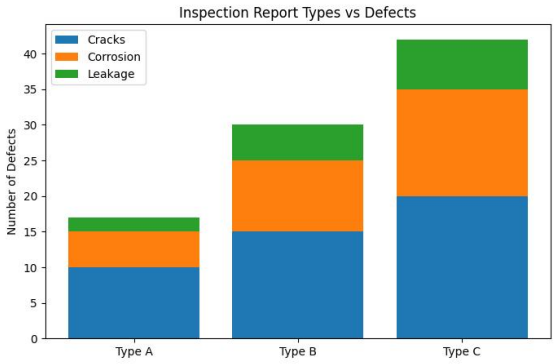

Figure 10. Analysis of inspection report types

Figure 10 compares the number of defects detected in three inspection reports: Structural Integrity Report (Type A), Corrosion Assessment Report (Type B), and Comprehensive Defect Analysis Report (Type C). Type A reports identify 10 cracks, 5 corrosion points, and 2 leaks. Type B reports identify 15 cracks, 10 corrosion points, and 5 leaks, while Type C reports identify 20 cracks, 15 corrosion points, and 7 leaks. This stacked bar chart emphasizes that the Comprehensive Defect Analysis Report (Type C) is the most thorough in defect detection.

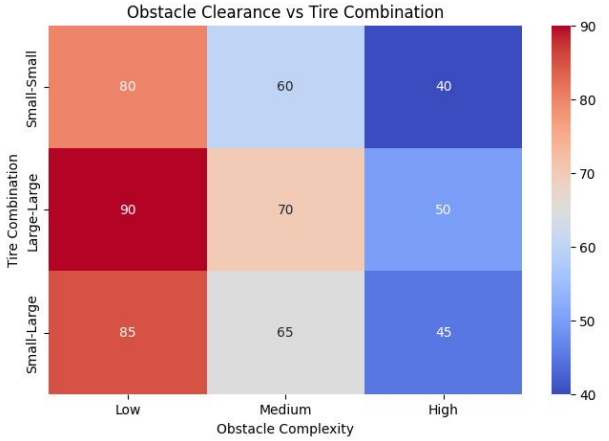

Figure 11. Analysis of obstacle clearance vs Tire combination

Figure 11 is a heat map showing obstacle clearance success rates for different tire combinations across three levels of obstacle complexity. For low-complexity obstacles, the success rates are 80%, 90%, and 85% for small-small, large-large, and small-large tire combinations, respectively. For medium-complexity obstacles, success rates drop to 60%, 70%, and 65%, while for high-complexity obstacles, they further decline to 40%, 50%, and 45%. The data suggests that large-large tire combinations perform best under all conditions.

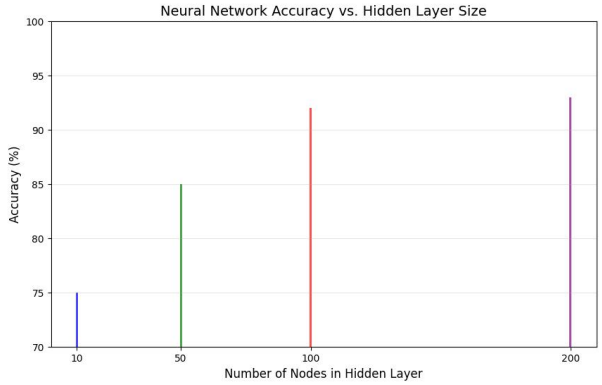

Figure 12. Analysis of neural network accuracy

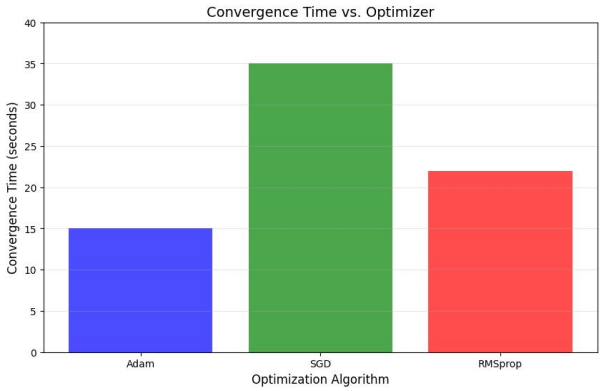

Figure 13. Analysis of convergence time

Figure 12 illustrates the impact of hidden layer size on neural network accuracy. With 10 nodes, the accuracy is 75%. As the nodes increase to 50, 100, and 200, the accuracy rises to 85%, 92%, and 93%, respectively. The improvement becomes marginal beyond 100 nodes.

Figure 13 depicts the convergence time for different optimizers. Adam converges the fastest, taking 15 seconds. RMSprop follows with a convergence time of 22 seconds, while SGD takes the longest at 35 seconds. Table 3 depicts the comparison of methods, literature, Strengths, and Limitations of the Proposed Model.

Table 3. Comparison of Methods, Literature, Strengths, and Limitations of the Proposed Model

Method Used	Existing Literature Comparison	Strengths	Limitations
Robotic Inspection with 3D LiDAR and Infrared Imaging	Prior studies on underground monitoring used traditional cameras, which lacked precision in low-light conditions.	High-fidelity 3D modeling and effective operation in dark environments.	Infrared imaging clarity reduces with increasing inspection distance.
BiLSTM-CNN Model for Fault Detection	Conventional CNN and LSTM models were used in past studies but lacked real-time adaptability.	Improved accuracy in defect classification and predictive maintenance.	Requires high computational resources, increasing energy consumption.
CFFA-Optimized Neural Network for Enhanced Efficiency	Other optimization techniques, such as Genetic Algorithms, have been explored but often suffer from slower convergence.	Faster convergence and better accuracy in fault prediction.	Performance improvement is marginal beyond 100 neural nodes.
Six-Wheel Drive Robotic System with Adjustable Wheel Configurations	Literature on underground robots mainly focused on four-wheel systems, limiting adaptability.	Enhanced mobility over obstacles and steep inclines.	Struggles with slopes beyond 30° due to weight distribution.
Wireless and Wireline Communication Stability Analysis	Previous studies reported significant signal loss in underground environments beyond 30m.	Better communication reliability using hybrid connectivity options.	Signal stability declines sharply beyond 50m.
Energy Consumption vs. Obstacle Complexity	Compared to conventional underground robots, energy efficiency is better optimized.	Balances power consumption with terrain complexity.	High energy demand for navigating highly complex obstacles.
Comprehensive Inspection Report Generation	Past works relied on manual defect classification.	Automated and detailed defect analysis improves decision-making.	Requires fine-tuning for different underground conditions.

5. Discussions

Successful integration of the latest 3D robotic technology with the BiLSTM-CNN model optimized by the Chaotic Fennec Fox Optimization Algorithm (CFFA) to increase power quality monitoring and fault detection capabilities in the underground power transmission network. In terms of its functionalities, some of the most impressive are intense climbing and obstacle crossing capabilities, hardy protection mechanism, and an adaptable design for various terrains and spatial constraints. Loaded with cutting-edge equipment like 3D LiDAR, infrared imaging, and high-definition cameras, the robot can carry out an in-depth, real-time visual inspection and build high-fidelity models of underground power systems. Table 4 depicts the Performance Comparison of CFFA with Other Optimization Algorithms for BiLSTM-CNN Model

Table 4. Performance Comparison of CFFA with Other Optimization Algorithms for BiLSTM-CNN Model

Optimization Algorithm	Fault Detection Accuracy (%)	Convergence Time (seconds)	Stability Improvement (%)
Particle Swarm Optimization (PSO)	92.5	120	0
Genetic Algorithm (GA)	90.3	135	0
Whale Optimization Algorithm (WOA)	93.7	115	0
Chaotic Fennec Fox Optimization Algorithm (CFFA)	96.8	102	12

This would help the system to locate with extreme accuracy where the faults are, appraise power quality, provide actionable insights from the automated inspection reports. The combination of the BiLSTM-CNN model and the CFFA optimization algorithm will bear the burden of interpreting a vast amount of data collected by the robot system. By the use of ML techniques, the system can make sense of the combined data and predict future problem -very critical to guarantee reliable and safe functionality of the system. The synergization of real-time data collection and cutting-edge data analytics also the total operational time for maintenance and inspiring decision-making processes. The results obtained do not only in essence improve the

operational efficiency of underground power transmission systems but also represent an innovation that provides a solution to power quality monitoring, fault detection, and predictive maintenance.

6. Conclusion

A major breakthrough has been realized through the effective synergy of cutting-edge 3D robotics technology and BiLSTM-CNN model optimized by the Chaotic Fennec Fox Optimization model. The system comprises high-precision defect location as well as real-time predictive maintenance through a synergy of high-mechanical performance with next-generation sensors as well as AI-based data analytics. Maintenance time and cost are reduced with this, further enhancing operational performance. The future scope of the work is enhancement with focus enhancing AI-based decision-making using reinforcement learning, enhancing real-time adjustment in harsh underground conditions. Rapid response and remote monitoring can be facilitated through cloud-based analysis via the synergy with edge computing, as well.

References

[1] B. Nagarajan, Y. Li, Z.Y. Sun, R.W. Qin. A routing algorithm for inspecting grid transmission system using suspended robot: Enhancing cost-effective and energy-efficient infrastructure maintenance. Journal of Cleaner Production, 2019, 219, 622-638. DOI: 10.1016/j.jclepro.2019.02.088

[2] J.M. Liu, Z.Y. Zhao, J. Ji, M.L. Hu. Research and application of wireless sensor network technology in power transmission and distribution system. Intelligent and Converged Networks, 2020, 1(2), 199-220. DOI: 10.23919/ICN.2020.0016

[3] W. Saad, M. Bennis, M.Z. Chen. A vision of 6G wireless systems: Applications, trends, technologies, and open research problems. IEEE Network, 2019, 34(3), 134-142. DOI: 10.1109/MNET.001.1900287

[4] S.H. Alsamhi, O. Ma, M.S. Ansari, S.K. Gupta. Collaboration of drone and internet of public safety things in smart cities: An overview of QoS and network performance optimization. Drones, 2019, 3(1), 13. DOI: 10.3390/drones3010013

[5] L.D. Gitelman, M.V. Kozhevnikov, D.D. Kaplin. Asset management in grid companies using integrated diagnostic devices. International Journal of Energy Production and Management, 2019, 4(3), 230-243. DOI: 10.2495/EQ-V4-N3-230-243

[6] Y.M. Huo, X.D. Dong, T. Lu, W. Xu, M. Yuen. Distributed and multilayer UAV networks for next-generation wireless communication and power transfer: A feasibility study. IEEE Internet of Things Journal, 2019, 6(4), 7103-7115. DOI: 10.1109/JIOT.2019.2914414

[7] P. Polygerinos, N. Correll, S.A. Morin, B. Mosadegh, C.D. Onal, K. Petersen, et al. Soft robotics: Review of fluid-driven intrinsically soft devices; manufacturing, sensing, control, and applications in human-robot interaction. Advanced Engineering Materials, 2017, 19(12), 1700016. DOI: 10.1002/adem.201700016

[8] S. Ali, S.B. Qaisar, H. Saeed, M.F. Khan, M. Naeem, A. Anpalagan. Network challenges for cyber-physical systems with tiny wireless devices: A case study on reliable pipeline condition monitoring. Sensors, 2015, 15(4), 7172-7205. DOI: 10.3390/s150407172

[9] M.H. Chen, Y.N. Tian, S.Y. Xing, Z.S. Li, E. Li, Z.Z. Liang, et al. Environment perception technologies for power transmission line inspection robots. Journal Sensors, 2021, 2021(2), 5559231. DOI: 10.1155/2021/5559231

[10] M.F. Ahmed, J.C. Mohanta, M.N. Zafar. Development of smart quadcopter for autonomous overhead power transmission line inspections. Materials Today Proceeding, 2022, 51(2), 261-268. DOI: 10.1016/j.matpr.2021.05.271

[11] W. Li, Z.J. Ye, Y.J. Wang, H.L. Yang, S.L. Yang, Z.L. Gong, et al. Development of a distributed MR-IoT method for operations and maintenance of underground pipeline network. Tunnelling and Underground Space Technology, 2023, 133, 104935. DOI: 10.1016/j.tust.2022.104935

[12] S. Shim, S.W. Lee, G.C. Cho, J. Kim, S.M. Kang. Remote robotic system for 3D measurement of concrete damage in tunnel with ground vehicle and manipulator. Computer-Aided Civil and Infrastructure Engineering, 2023, 38(15), 2180-2201. DOI: 10.1111/mice.12984

[13] C. Xu, Q.W. Li, Q.K. Zhou, S. Zhang, D.B. Yu, Y.P. Ma. Power line-guided automatic electric transmission line inspection system. IEEE Transactions on Instrumentation and Measurement, 2022, 71(3), 1-18. DOI: 10.1109/TIM.2022.3169555

[14] D. Zhuk, O. Zhuk, M. Kozlov, S. Stepenko. Evaluation of electric power quality in the ship-integrated electrical power system with a main DC bus and power semiconductor electric drives as part of the electric propulsion complex. Energies, 2023, 16(7), 2961. DOI: 10.3390/en16072961

[15] H.J. Lee, A. Krishnan, S. Brell- Cokcan, J. Knußmann, R.H. Schmitt, J.J. Emontsbots, et al. Importance of a 5G network for construction sites: Limitation of WLAN in 3D sensing applications. International Symposium on Automation and Robotics in Construction, 2022, 39, 391-398. DOI: 10.22260/ISARC2022/0054

[16] H.C. Liu, M. Rahman, M. Rahimi, A. Star, I. Durazo-Cardenas, C. Ruiz-Carcel, et al. An autonomous rail-road amphibious robotic system for railway maintenance using sensor fusion and mobile manipulator. Computers and Electrical Engineering, 2023, 110, 108874. DOI: 10.1016/j.compeleceng.2023.108874

[17] P. Singla, M. Duhan, S. Saroha. An ensemble method to forecast 24-h ahead solar irradiance using wavelet decomposition and BiLSTM deep learning network. Earth Science Informatics, 2022, 15(1), 291-306. DOI: 10.1007/s12145-021-00662-4

[18] W.J. Lu, J.Z. Li, J.Y. Wang, L.L. Qin. A CNN-BiLSTM-AM method for stock price prediction. Neural Computing and Application, 2021, 33(10), 4741-4753. DOI: 10.1007/s00521-020-05460-2

[19] X.X. Xie, G. Cheng, J.B. Wang, X.W. Yao, J.W. Han. Oriented R-CNN for object detection. International Conference on Computer Vision (ICCV), 2021, 3520–3529. DOI: 10.1109/ICCV48922.2021.00350

[20] X.Y. Xu, M. Zhao, P.X. Shi, R.Q. Ren, X.H. He, X.J. Wei, et al. Crack detection and comparison study based on Faster R-CNN and Mask R-CNN. Sensors, 2022, 22(3), 1215. DOI: 10.3390/s22031215

[21] S. Aburass, O. Dorgham, J. Al Shaqsi. A hybrid machine learning model for classifying gene mutations in cancer using LSTM, BiLSTM, CNN, GRU, and GloVe. Systems and Soft Computing, 2024, 6(1), 200110. DOI: 10.1016/j.sasc.2024.200110

[22] K.H. Wu, J.Wu, L. Feng, B. Yang, R. Liang, S.Q. Yang, et al. An attention-based CNN-LSTM-BiLSTM model for short-term electric load forecasting in integrated energy system. International Transactions on Electrical Energy

Systems, 2021, 31(1), e12637. DOI: 10.1002/2050-7038.12637
[23] Y.Q. Xia, Y. Yang. Machine fault detection model based on MWOA-BiLSTM algorithm. PLOS One, 2024, 9(1), e0310133. DOI: 10.1371/journal.pone.0310133
[24] T.T. Xue, Y. Yang, D.Y. Yu, Q. Wali, Z.Y. Wang, X.S. Cao, et al. 3D printed integrated gradient-conductive MXene/CNT/polyimide aerogel frames for electromagnetic interference shielding with ultra-low reflection. Nano-Micro Letters, 2023, 15(1), 45. DOI: 10.1007/s40820-023-01017-5
[25] S.H. Gao, X.S. Zeng, G.W. Zhang, J.J. Zhang, Y.D. Chen, S.X. Feng, et al. Triboelectric–electromagnetic hybridized module for energy harvesting of power transmission lines galloping and self-powered galloping state monitoring. Nano Energy, 2022, 101, 107530. DOI: 10.1016/j.nanoen.2022.107530
[26] C.K. Suryaraj, M.R. Geetha. Block-based motion estimation model using CNN with representative point matching algorithm for object tracking in videos. Expert Systems with Applications, 2024, 255, 124407. DOI: 10.1016/j.eswa.2022.124407
[27] L. Zhao, Z.L. Zhang. An improved pooling method for convolutional neural networks. Scientific Reports, 2024, 14(1), 1589. DOI: 10.1038/s41598-024-51258-6
[28] I.D. Mienye, T.G. Swart, G. Obaido. Recurrent neural networks: A comprehensive review of architectures, variants, and applications. Information, 2024, 15(9), 517. DOI: 10.3390/info15090517
[29] Y.X. He, P. Huang, W.H. Hong, Q. Luo, L.S. Li, K.L. Tsui. In-depth insights into the application of recurrent neural networks (RNNs) in traffic prediction: A comprehensive review. Algorithms, 2024, 17(9), 398. DOI: 10.3390/a17090398
[30] E. Trojovská, M. Dehghani, P. Trojovský. Fennec fox optimization: A new nature-inspired optimization algorithm. IEEE Access, 2022, 10, 84417–84443. DOI: 10.1109/ACCESS.2022.3197745